ELSEVIER

Materials Science and Engineering A 427 (2006) 348–355

MATERIALS SCIENCE & ENGINEERING A

www.elsevier.com/locate/msea

Theoretical investigation of wear-resistance mechanism of superelastic shape memory alloy NiTi

Wenyi Yan *

School of Engineering and Information Technology, Deakin University, Geelong, Vic. 3217, Australia

Received 1 February 2006; received in revised form 23 April 2006; accepted 4 May 2006

Abstract

Recent experimental research indicates that superelastic shape memory alloy nickel–titanium (NiTi) is superior to stainless steel against wear and could be applied in tribological engineering. It is believed that the super wear resistance of shape memory alloys is mainly due to the recovery of the superelastic deformation. Our recent wear study indicates that wear rate is very sensitive to the maximum contact pressure. In the present investigation, which involves applying Hertz contact theory and the finite element method, the wear behaviour of shape memory alloys is examined against that of stainless steels through analyzing the maximum contact pressure and the plastic deformation. Our investigation indicates that the contribution of superelasticity to the high wear resistance of NiTi is directly linked to the low transformation stress and the large recoverable transformation strain. Furthermore, the low Young's modulus of this alloy also plays an important role to reduce the maximum contact pressure and therefore reduce the wear rate. Additionally, the high plastic yield strength of transformed martensite NiTi enhances its wear resistance further.

Keywords: Shape memory alloys; Phase transformation; Wear; Theory and modeling; Contact mechanics

1. Introduction

Shape memory alloys (SMAs) are well known for possessing shape memory effect and superelasticity behaviour due to intrinsic microstructure transition of thermoelastic martensitic transformation. Both shape memory effect and superelasticity have been exploited to design functional and smart structures in mechanical and biomedical engineering [1–3]. A number of commercial products are already available on the market. For instance, couplings and fasteners based on shape memory effect have been extensively developed and applied. A historical example is the large-scale application of SMAs coupling to connect titanium hydraulic tubing in the aircraft F-14 in 1971 [4].

Many more potential applications and mechanical behaviours of SMAs have been investigated. For example, an anomalous relationship between hardness and wear properties of a superelastic NiTi alloy was reported by Qian et al. [5] through their microwear tests. Some other indentation studies on NiTi can be found in [6–9]. Recently, several experimental wear studies of SMAs indicate that SMAs are superior to common wear-resistant materials against wear. Richman et al. [10] discovered from their experimental tests that NiTi alloys, a typical SMA, are much more resistant to cavitation erosion than even the best stainless steels. Jin and Wang [11] discovered in their experiments that the sliding wear resistance of NiTi is better than that of nitrided 38CrMoA1A alloy steel. The high wear resistance of this alloy is believed to be mainly due to its superelasticity or pseudoelasticity. For instance, Jin and Wang [11] believed that one of the reasons for the high wear resistance is that NiTi has high reversible strain ability. Li [12,13] stated that the high wear resistance of NiTi alloy is mainly attributed to its unique pseudoelasticity.

If the recovery of the large deformation due to forward and reverse transformation, i.e. superelasticity, is the major reason for the high wear resistance of austenite NiTi, then it can be expected that martensite NiTi, which could not demonstrate superelastic behaviour, would have poorer wear behaviour. However, experimental study indicates that martensite NiTi has similar erosion wear behaviour to austenite NiTi, which could demonstrate superelasticity [10]. This experimental result implicates that superelasticity might not be the only reason for the high wear resistance of NiTi. Liang et al. [14] pointed out, "it therefore seems unreasonable to emphasize simply the role of pseudoelasticity in wear behaviour of NiTi alloys".

* Tel.: +61 3 52272082; fax: +61 3 52272167.
E-mail address: wenyi.yan@deakin.edu.au.

0921-5093/$ – see front matter © 2006 Elsevier B.V. All rights reserved.
doi:10.1016/j.msea.2006.05.005

From the solid mechanics point of view, wear of metallic materials, defined as the removal of material from surface due to cyclic mechanical contact either from sliding contact in adhesive and abrasive wear or particle impulsion in erosion wear, originates from plastic deformation [15–17]. Plastic deformation and accumulation of plastic deformation due to cyclic loading will initiate microcracks in the surface and eventually wear debris will form. Therefore, the wear resistance of a ductile material can be evaluated by its capacity of plastic deformation under wearing conditions. Under given contact loading conditions, if plastic deformation is difficult to be generated in a material, then this material is expected to possess a high wear resistance.

Generally, in a contact problem, the maximum contact pressure instead of the total contact force will directly determine the maximum stress to trigger plastic deformation. For example, the maximum shear stress is equal to 0.3 of the maximum contact pressure in a plane strain contact problem between two cylindrical bodies [18]. Therefore, the maximum contact pressure can be used to evaluate the initiation of plastic deformation in materials. Based on the wear mechanism of plastic accumulation and micromechanics analysis, a computation-based wear model was established [17]. According to this model, the wear rate under sliding condition is very sensitive to the maximum contact pressure. We can compare the wear behaviours of NiTi SMA and stainless steel by investigating the maximum contact pressure under given applied loads. In this paper, the maximum contact pressures are obtained from both Hertz contact theory for elastic contact and finite element analysis for elastic–transformation–plastic contact. The major factors attributed to the high wear resistance of NiTi are discussed based on the results obtained.

2. Ratcheting-based wear model for metallic materials

To understand the effect of the maximum contact pressure on the wear rate, the wear model developed in [17] is briefly discussed in this section. Sliding wear in a ductile material generally involves three steps, as illustrated in Fig. 1. Initially (see Fig. 1a), localized deformation patterns develop beneath the contacting surface as a result of the sliding contact loads [19–21]. Such localized deformation can be the precursor of microcracks, which form as a result of the coalescence of microvoids nucleated at inclusions in highly deformed regions at the subsurface, as shown in Fig. 1b. Continued sliding contact promotes crack growth and causes neighbouring cracks to coalesce (Fig. 1c). Eventually, cracks propagate towards the surface at weak points and wear debris is formed.

Kapoor and Johnson [15] have analyzed the formation of debris during sliding wear tests and proposed the repeated accumulation of plastic strain, or ratcheting, as the mechanism leading to sliding wear in metals. The ratcheting phenomena were well observed in sliding wear tests [22]. Yan et al [17] applied the finite element method to study the plastic deformation due to cyclic sliding contact. The accumulation of plastic strain, i.e. ratcheting, was successfully simulated as shown in Fig. 2. In this case, both plastic strain components ε_{11}^{p} and ε_{12}^{p}, normalized by the yield strain ε_y, beneath the surface at a depth b increase during the cyclic sliding contact process in the large deformation analysis. Under the contact sliding condition, the accumulation of plastic shearing strain is obviously more significant. Here the ratcheting strain is defined as the increase in strain per loading cycle, denoted as $\delta\varepsilon_{11}^{p}$ and $\delta\varepsilon_{12}^{p}$ for the normal- and shear-strain components, respectively, in Fig. 2. The results show that these quantities remain almost constant after about the first 10 sliding cycles.

Following the analogy with multiaxial fatigue [23], an effective plastic strain was introduced in terms of the individual components of plastic strains ε_{ij}^{p} as follows:

$$\varepsilon_{\text{eff}} = \sqrt{\frac{2}{3}\varepsilon_{ij}^{p}\varepsilon_{ij}^{p}}. \quad (1)$$

Therefore, the ratcheting rate in this multiaxial ratcheting phenomenon can be represented by the increase of the effective plastic strain per cycle $\delta\varepsilon_{\text{eff}}$.

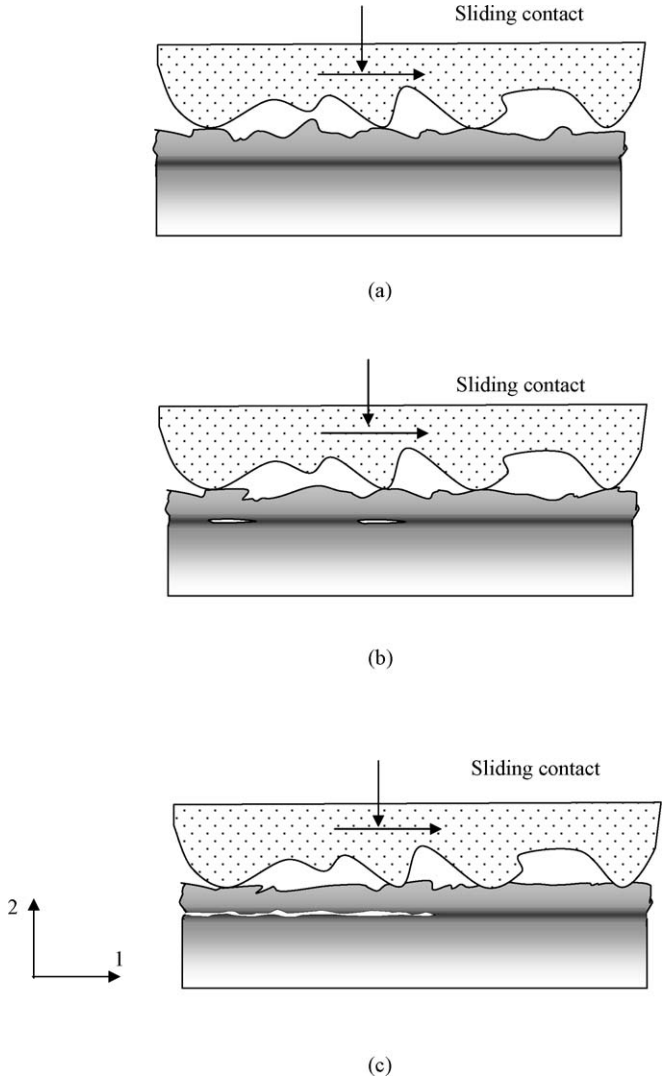

Fig. 1. Schematic representation of a sliding wear process: (a) accumulated plastic deformation in the subsurface, darker regions correspond to higher levels of accumulative plastic strains; (b) subsurface crack initiation; (c) crack propagation and wear debris formation [17].

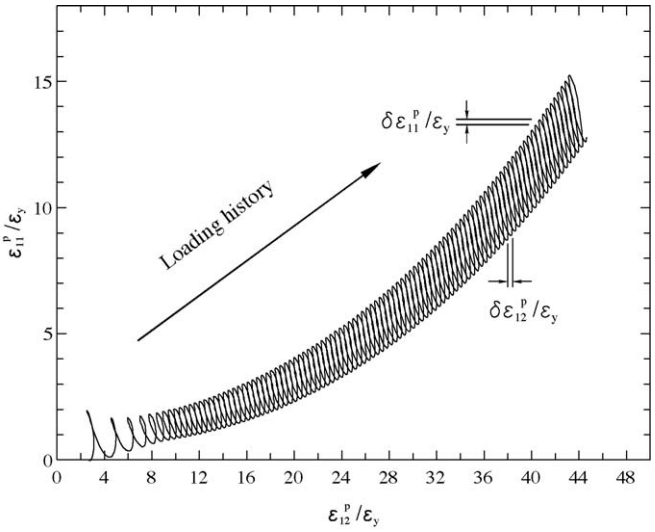

Fig. 2. Accumulation of plastic strains at a depth b beneath a sliding contact surface during a ratcheting state [17].

For ratcheting, the local failure of the material can be assumed to occur by a ductile mechanism linked to the exhaustion of the local ductility of the material [24]. In such cases, local failure may be controlled by the accumulation of an appropriate plastic strain measure per cycle with failure occurring when it reaches the ductility of the material, ε_f. Based on this ratcheting failure mechanism, the number of sliding cycles to failure due to ratcheting can be estimated as:

$$N_f = \frac{\varepsilon_f}{\delta\varepsilon_{eff}}. \tag{2}$$

If materials fail at the depth b, which can be determined from numerical simulation, the wear rate can be derived as [17]:

$$W = \frac{\delta\varepsilon_{eff} b}{\varepsilon_f}. \tag{3}$$

This wear model was successfully applied to evaluate the wear behaviour of a coated component [25]. It can also be applied to study the influences of some key parameters on the sliding wear. For example, according to this model, the wear rate under sliding condition is very sensitive to the maximum contact pressure. Fig. 3 shows the variation of the normalized wear rate, $W\varepsilon_f/l$, with the normalized maximum contact pressure, p_0/k_c, where k_c is the shear strength of the material. The wear rate increases dramatically when the maximum pressure p_0 increases from 3.75 to 4.5 times of the shear strength. Therefore, the maximum pressure instead of the total applied load is a key variable to initiate plastic deformation and to evaluate the wear rate. Here, the maximum pressure can be considered as an indicator of the intensity of the applied load. Generally speaking, the intensity of the applied load, such as stress, instead of the applied load itself will eventually determine the failure of a material.

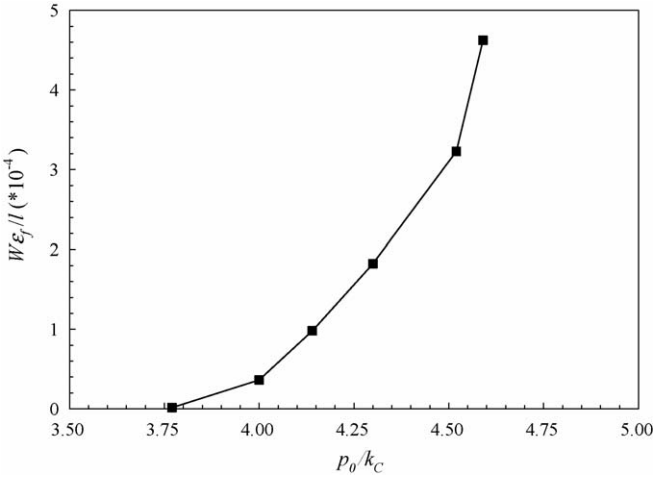

Fig. 3. Influence of the maximum contact pressure on the sliding wear rate.

3. Examination based on Hertz theory

A simplified two-dimensional plane-strain contact model is shown in Fig. 4 to simulate the mechanics action of a sliding wear process. At microscale the surfaces are contacted through asperities due to the roughness of the surfaces. The rigid cylinder in Fig. 4 represents a hard asperity, which is subjected to an applied per unit thickness force F and contacts a semi-infinite body. The semi-infinite body represents NiTi or steel with the elastic modulus of E and Poisson's ratio of ν.

According to Hertz theory of elastic contact, the maximum pressure is:

$$p_0 = \left(\frac{FE^*}{\pi R}\right)^{1/2} \tag{4}$$

where R is the radius of the rigid asperity and $E^* = E/(1-\nu^2)$. The Poisson's ratios of a NiTi alloy and a steel can be reasonably assumed as the same. Therefore, the maximum contact pres-

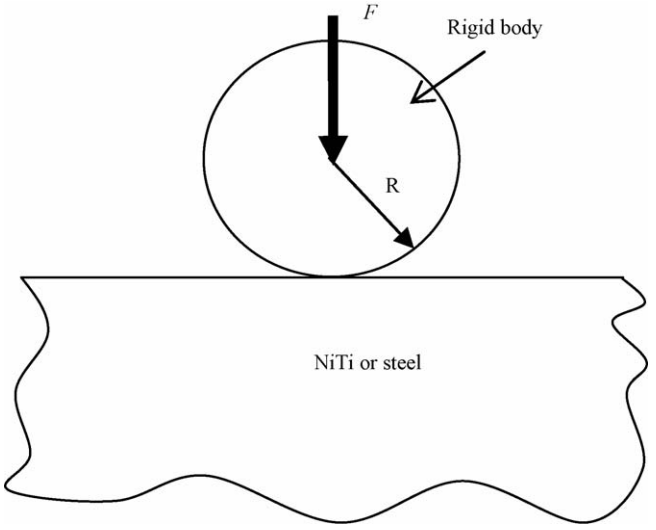

Fig. 4. Illustration of a rigid asperity contacting a NiTi alloy or a steel.

sure is proportional to the square root of the Young's modulus, i.e.:

$$p_0 \propto (E)^{1/2} \tag{5}$$

The Young's modulus of a steel is about 200 GPa while it is much lower for NiTi alloys. For example, a value of only 60 GPa for the Young's modulus of a superelastic NiTi can be estimated from a uniaxial test in [26]. Therefore, under the same applied force and the same contact geometry, the maximum pressure in NiTi alloy is about 0.55 of the maximum pressure in a typical steel from this simple Hertz elastic contact analysis. The lower maximum pressure delays the plastic deformation in NiTi alloy, which contributes to the increase in the wear resistance of this material. Bear in mind, a low Young's modulus can be a factor against wear but not the sole factor. One cannot jump to the conclusion that a low Young's modulus will necessarily lead to a high wear resistance. Incorporating the influence of Young's modulus, some investigators proposed to use the ratio of hardness to elastic modulus as a parameter for predicting wear resistance, e.g. [27,28].

4. Examination based on elastic–plastic analysis

4.1. Finite element model

In the previous section, we used Hertz theory to analyze the maximum contact pressure for a typical NiTi alloy and a typical steel alloy. Strictly, Hertz theory is only suitable for elastic materials. During a wear process, the material within the failure zone will certainly be in plastic state either for a steel or a NiTi. In the case of superelastic austenite NiTi alloys, prior to plastic deformation, the material will experience forward austenite-to-martensite transformation, which accompanies a large deformation. Therefore, plastic deformation in steel and the deformation due to martensitic transformation plus plastic deformation in NiTi should be considered in order to get the accurate results of the maximum contact pressure during a wear process. Here the numerical finite element method is utilized to simulate the contact problems, elastic–plastic contact for steel and elastic–transformation–plastic contact for NiTi.

The geometrical model is the same as the one shown in Fig. 4. The radius R of the rigid body is chosen as 0.4 mm to represent the size of a typical asperity. The finite element model is shown in Fig. 5. Here a plane-strain problem is considered to simulate the contact between a rigid cylinder and a semi-infinite NiTi or stainless steel. Due to symmetry, only a half of the geometrical model is simulated. A total of 1940 four-node quadrilateral elements are employed in the finite element model. A fine mesh is built near the contacting surface.

4.2. Material data and material models

A typical NiTi superelastic alloy from [26] is considered in the current investigation. As shown by the solid line in Fig. 6, in the uniaxial tensile test for superelasticity, a large strain of over 4% due to austenite-to-martensite forward transformation can be recovered during the unloading martensite-to-austenite reverse transformation process. If the load is increased continuously after the full forward transformation, as indicated by the dashed line in Fig. 6, the martensite of the NiTi alloy will have normal plastic deformation until it fails. The uniaxial tensile stress–strain curve of a typical stainless steel alloy (UNS31803) from [29] is also plotted by the dash-dotted line in Fig. 6. If the load is increased continuously, the tensile steel bar will experience elastic deformation, plastic deformation and eventually breaking. The basic material data for the steel and the NiTi alloy are summarized in Table 1, which are applied in the finite element calculations.

In our simulation, the plasticity of the steel is treated as normal isotropic hardening based on von Mises yield criterion. A

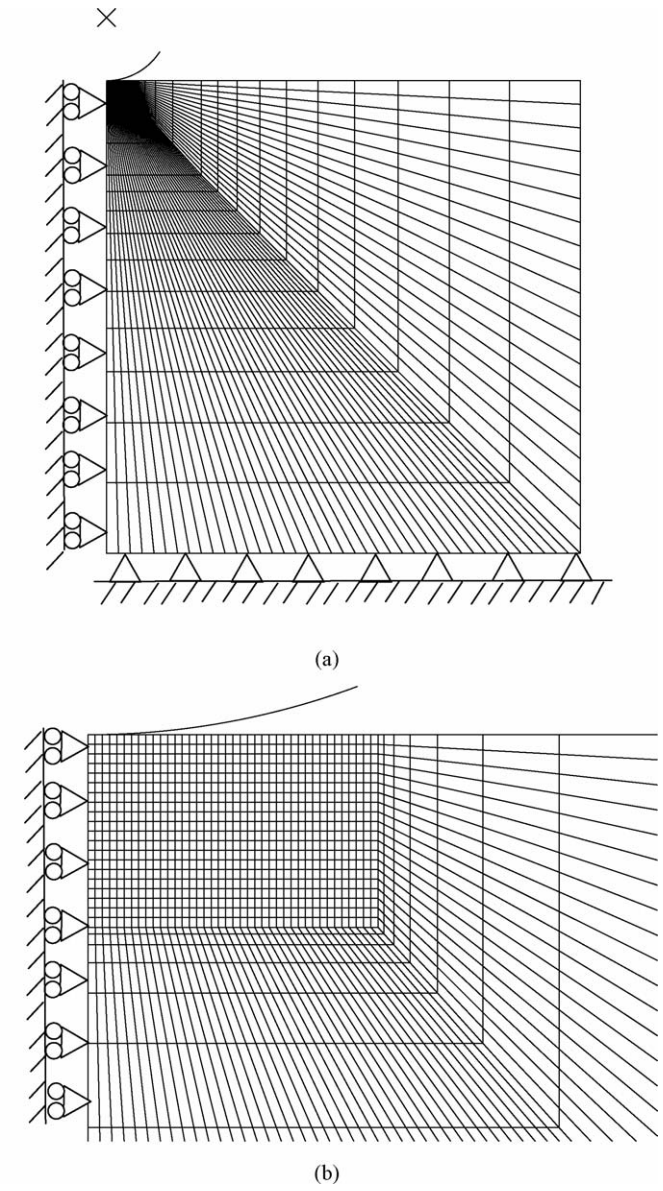

Fig. 5. Finite element model for the elastic–plastic contact simulations: (a) the entire finite element mesh and boundary conditions; (b) the fine mesh near the contact zone.

Table 1
Basic material data for the NiTi alloy [26] and the stainless steel [29]

Alloy	Young's modulus (GPa)	Transformation stress (MPa)	Yield strength (MPa)	Ultimate strength (MPa)
NiTi	62	407	1058	1330
Stainless steel	200	–	575	805

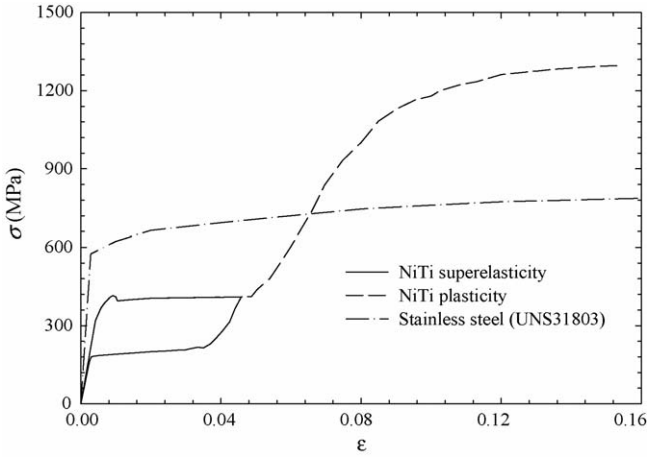

Fig. 6. Superelasticity and superelastic–plastic deformation of a NiTi alloy and elastic–plastic deformation of a stainless steel.

combined transformation plus plasticity model developed by Yan et al. [30] is utilized in the present investigation to describe the stress–strain relationship of the superelastic NiTi. Now, the total strain rate of the superelastic material generally composes of three parts:

$$\dot{\boldsymbol{\varepsilon}} = \dot{\boldsymbol{\varepsilon}}^{\mathrm{el}} + \dot{\boldsymbol{\varepsilon}}^{\mathrm{tr}} + \dot{\boldsymbol{\varepsilon}}^{\mathrm{pl}} \tag{6}$$

where $\dot{\boldsymbol{\varepsilon}}^{\mathrm{el}}$ is the elastic strain rate due to elastic deformation, $\dot{\boldsymbol{\varepsilon}}^{\mathrm{tr}}$ the transformation strain rate due to transformation and $\dot{\boldsymbol{\varepsilon}}^{\mathrm{pl}}$ the plastic strain rate due to dislocation movement. Plastic deformation due to dislocation movement is unrecoverable, whereas elastic and transformation deformation are recoverable. The elastic strain rate $\dot{\boldsymbol{\varepsilon}}^{\mathrm{el}}$ is controlled by the isotropic Hooke's law. The transformation strain rate $\dot{\boldsymbol{\varepsilon}}^{\mathrm{tr}}$, which is proportional to the martensite volume fraction, is described by a reversible transformation model. The isotropic hardening theory based on von Mises yield condition can be applied to describe the plastic strain rate $\dot{\boldsymbol{\varepsilon}}^{\mathrm{pl}}$. Recent experimental results indicate that plastic deformation in superelastic NiTi can hinder the reverse transformation [26]. This constraint effect can be realized by introducing a stabilized irrecoverable martensite volume fraction f_{sta}. Quantitatively, f_{sta} is assumed to be dependent on the level of prior plastic strain, i.e.:

$$f_{\mathrm{sta}} = F(\bar{\varepsilon}^{\mathrm{pl}}) \tag{7}$$

where $\bar{\varepsilon}^{\mathrm{pl}}$ is the equivalent plastic strain. A linear relation given below would be the simplest one between f_{sta} and $\bar{\varepsilon}^{\mathrm{pl}}$:

$$f_{\mathrm{sta}} = \begin{cases} \dfrac{\bar{\varepsilon}^{\mathrm{pl}}}{\bar{\varepsilon}_{\mathrm{c}}^{\mathrm{pl}}}, & \bar{\varepsilon}^{\mathrm{pl}} \le \bar{\varepsilon}_{\mathrm{c}}^{\mathrm{pl}} \\ 1, & \bar{\varepsilon}^{\mathrm{pl}} > \bar{\varepsilon}_{\mathrm{c}}^{\mathrm{pl}} \end{cases} \tag{8}$$

where $\bar{\varepsilon}_{\mathrm{c}}^{\mathrm{pl}}$ is the minimum equivalent plastic strain after which no reverse transformation will occur at all. Detailed discussion about this combined transformation and plasticity model can be found in [30].

4.3. Numerical results

Fig. 7 shows the numerical results of the maximum contact pressure as a function of the applied contact force for both the stainless steel and the NiTi alloy. It is clear to see that the maximum contact pressure, p_0, is smaller in the NiTi than in the stainless steel until the applied force is over about 140 N/mm or until the value of p_0 is over 1700 MPa. Such a high contact pressure corresponds to a severe sliding wear in steel. Therefore, the maximum contact pressure in the steel, in most sliding wear cases, will be much higher than that in the NiTi alloy, which might contribute higher wear rate in the steel based on the wear model of plastic deformation accumulation as discussed in Section 2. In the elastic contact region, as discussed in previous section, the lower Young's modulus of NiTi contributes to the lower maximum contact pressure in the NiTi. In the region above the elastic contact, referring to Table 1, the transformation stress of 407 MPa for the NiTi is lower than the yield strength of 575 MPa for the steel. Furthermore, as shown in Fig. 6, a large deformation with close to zero hardening occurs during the forward transformation. These are the two reasons for the NiTi to have a lower contact pressure under the same loading condition once the load is over the elastic limit. In other words, the effect of the superelasticity of NiTi on the maximum contact pressure is represented by the influences of the forward transformation stress and the amount of the recoverable transformation strain, both of which should be considered explicitly.

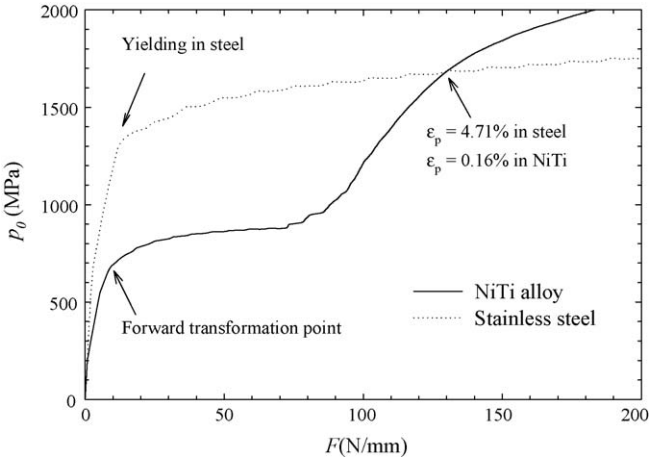

Fig. 7. Variation of the maximum contact pressure with the applied contact force from *FE* simulations for the elastic–plastic stainless steel and the superelastic–plastic NiTi alloy.

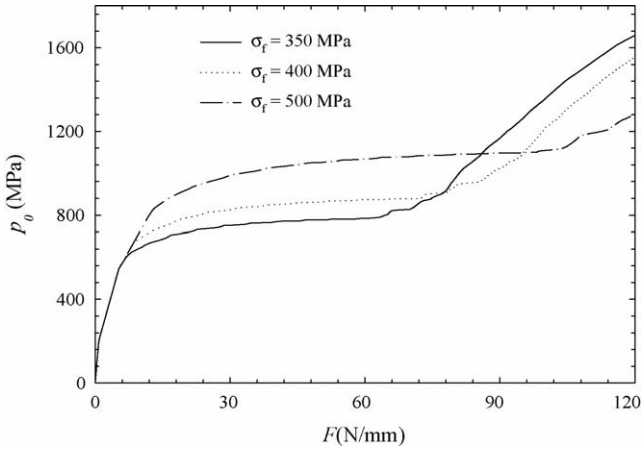

Fig. 8. Variation of the maximum contact pressure with the applied contact force for superelastic–plastic NiTi alloys with different forward transformation stresses.

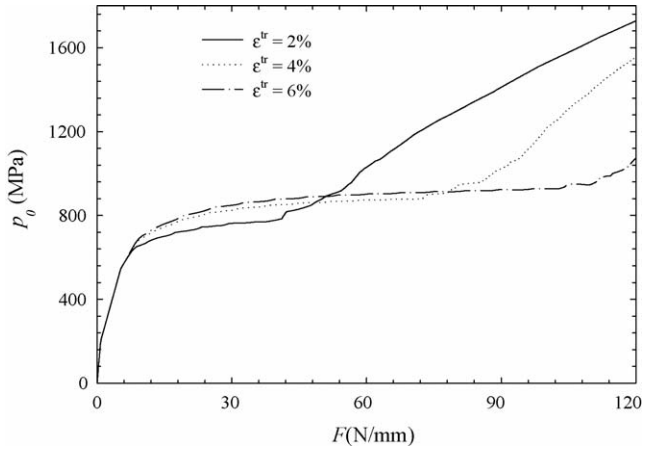

Fig. 9. Variation of the maximum contact pressure with the applied contact force for superelastic–plastic NiTi alloys with different recoverable transformation strains.

The influence of the forward transformation stress σ_f on the maximum contact pressure p_0 is demonstrated in Fig. 8. Here, the contact simulations were carried out for three NiTi superelastic alloys with different values of σ_f while all the other material data are the same as the one shown in Fig. 6. Following the loading path, we can see that each curve experiences three stages with obviously changed slopes, i.e. steep, flat and then climbing-up, which roughly corresponds to austenite elastic stage, transformation stage and martensite elastic–plastic stage, respectively. Fig. 8 indicates that the maximum contact pressure p_0 corresponding to the lowest σ_f of 350 MPa is much lower than any other case if the applied force is within the range of 20–65 N/mm, which roughly corresponds to the transformation stage of the alloy with $\sigma_f = 350$ MPa. Here, we can say "roughly" because small plastic deformation occurs at the end of this stage. If we compare the two cases of $\sigma_f = 400$ and 500 MPa, then we can find that p_0 is smaller for $\sigma_f = 400$ MPa as long as the applied load is smaller than 95 N/mm. Therefore, the maximum contact pressure decreases with the decrease of the forward transformation stress under mild contact loading condition. If the contact force is considerably large, we will have an opposite conclusion. The maximum contact pressure will be higher in the alloy with a lower forward transformation stress. For example, if F is larger than 95 N/mm, then p_0 will be larger in the alloy with $\sigma_f = 400$ MPa than that with $\sigma_f = 500$ MPa. The reason is that the forward transformation in the contact zone finishes earlier in the alloy with a lower σ_f and the structure becomes stiff earlier due to the following elastic deformation of the martensite.

The influence of the recoverable transformation strain ε^{tr} on the maximum contact pressure p_0 is demonstrated in Fig. 9. In the three contact simulations, the recoverable transformation strain ε^{tr} varies from 2 to 6% for the three superelastic NiTi SMAs while the other material properties are the same as the one shown in Fig. 6. We can see that within the transformation stage, i.e. the stage with flat slope, the difference of the maximum contact pressure p_0 is quite small between the three cases. The lowest p_0 corresponds to the smallest ε^{tr} within this stage. This might be due to the fact that the alloy with the smallest ε^{tr} has the largest transformation zone, which results in the slightly softest structure. The smaller the recoverable transformation strain ε^{tr} is, the earlier the alloy finishes the forward transformation stage, i.e. the earlier the alloy starts the martensite elastic–plastic stage, which signals the climbing of the p_0 versus F curve in Fig. 9. Therefore, the alloy with the largest transformation strain ε^{tr} has the largest domain of applied force F with a low maximum contact pressure p_0.

To sum up, the effect of the superelasticity of NiTi on the maximum contact pressure is represented by the influences of the forward transformation stress and the amount of the recoverable transformation strain. A low forward transformation stress leads to an early start of forward transformation, which corresponds to a low maximum contact pressure. On the other hand, a large recoverable transformation strain will result in a large loading domain with a low maximum contact pressure. One can predict that an alloy with a low forward transformation stress and a large recoverable transformation strain will lead to a low maximum contact pressure covering the stages of the forward transformation and the martensite elastic–plastic deformation, which implies a high wear resistance. This prediction is confirmed by the numerical curves in Fig. 10. Here, the alloy with the largest recoverable transformation strain of $\varepsilon^{tr} = 6\%$ and the lowest forward transformation stress of $\sigma_f = 350$ MPa has the lowest value of the maximum contact pressure in the entire range of the applied external force except the initial austenite elastic stage.

Now come back to the comparison of the superelastic–plastic NiTi and the stainless steel for the cases depicted in Fig. 7. Fig. 11 shows the comparison of the contact area radii, a, from the NiTi and the stainless steel. As we can expect, the contact area for the NiTi is significantly larger than that for the stainless steel for a given contact force in the entire loading range, which is consistent with the lower maximum contact pressure in the NiTi due to the lower transformation stress and a large transformation strain.

Fig. 12 shows the variations of the maximum equivalent plastic strains in the NiTi and the stainless steel with the applied contact force. It clearly indicates that the maximum equivalent

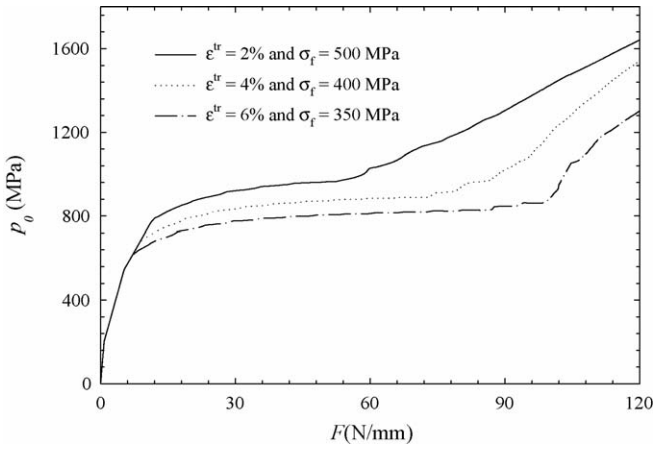

Fig. 10. Variation of the maximum contact pressure with the applied contact force for three superelastic–plastic NiTi alloys with different recoverable transformation strains and different forward transformation stresses.

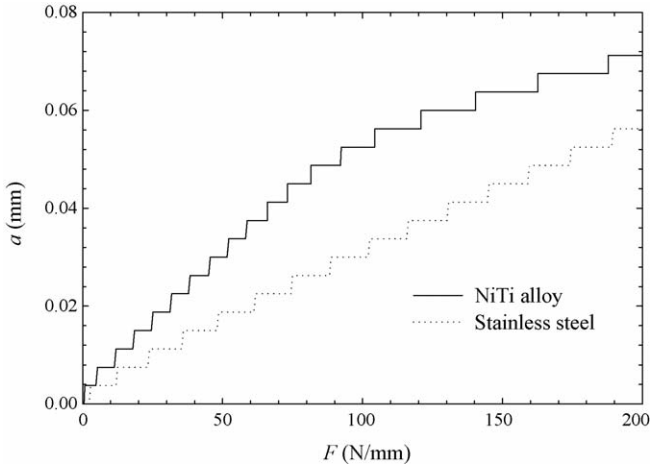

Fig. 11. Variation of the radius of the contact area with the applied contact force from *FE* simulations for the elastic–plastic stainless steel and the superelastic–plastic NiTi alloy.

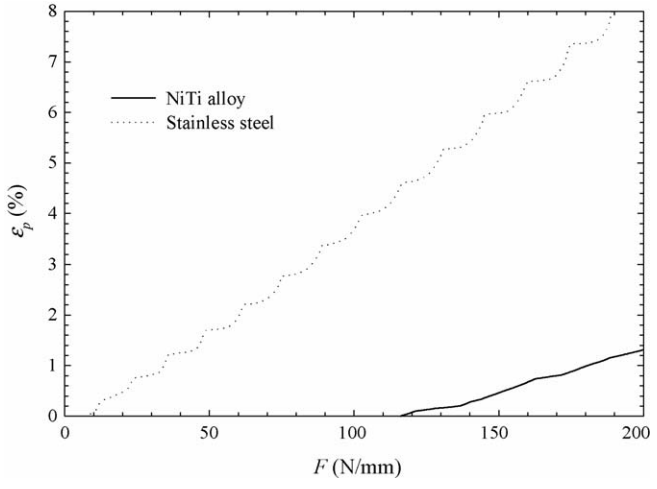

Fig. 12. Variation of the maximum equivalent plastic strain with the applied contact force from *FE* simulations for the elastic–plastic stainless steel and the superelastic–plastic NiTi alloy.

plastic strain is much lower in the NiTi in the entire loading range. The maximum plastic strain is over 4% in the steel when plastic deformation starts to occur in the NiTi. Referring to Fig. 7, at the point of equal maximum contact pressures in the NiTi and in the steel, our numerical results indicate that the steel close the contacting surface experiences significant plastic deformation with the maximum equivalent plastic strain of 4.71% while it is only 0.16% in the NiTi, which is in the early stage of yielding. Consequently, the steel close to the contacting surface is expected to fail earlier than the NiTi under such cyclic contact conditions in a wear test, considering NiTi possessing comparable ductility. The lower plastic deformation in the NiTi is due to the higher yield strength of the transformed martensite, which is 1058 MPa against 575 MPa for the steel as shown in Table 1.

5. Conclusions

Based on the wear model of plastic deformation accumulation, the wear rate is very sensitive to the maximum contact pressure. A higher maximum contact pressure would lead to a higher wear rate for the same material or materials with similar ductility. The maximum contact pressure in a typical superelastic NiTi alloy and in a typical stainless steel is examined by using Hertz elastic contact theory and the finite element method. Our results clearly indicate that a lower Young's modulus results in a lower contact pressure in the NiTi within the elastic contact limit. Beyond the elastic contact limit, the fact that the transformation stress in the NiTi is lower than the yield stress of the stainless steel will also result in a lower contact pressure in a typical wear test. Our numerical results also indicate that the high plastic yield stress of the transformed martensite in NiTi will hinder the occurrence of the plastic deformation and therefore increase the wear resistance of this material further. This investigation clearly demonstrates that the high wear-resistance of NiTi is due to the combined effects of low Young's modulus, low transformation stress, large recoverable transformation strain and high plastic yield strength of the martensite.

Acknowledgements

The finite element simulations were carried out at the National Facility of the Australian Partnership for Advanced Computing. The author is grateful to the unknown reviewer for his/her helpful comments for improving the manuscript.

References

[1] H. Funakubo, Shape Memory Alloys, Gordon and Bleach, New York, 1987.
[2] J. Van Humbeeck, Mater. Sci. Eng. A 273–275 (1999) 134–148.
[3] T. Duerig, A. Pelton, D. Stoeckel, Mater. Sci. Eng. A 273–275 (1999) 149–160.
[4] K.N. Melton, in: K. Otsuka, C.M. Wayman (Eds.), Shape Memory Materials, Cambridge University Press, Cambridge, UK, 1988, pp. 220–239.
[5] L. Qian, X. Xiao, Q. Sun, T. Yu, Appl. Phys. Lett. 84 (2004) 1076–1078.
[6] K. Gall, K. Juntunen, H.J. Maier, H. Sehitoglu, Y.I. Chumlyakov, Acta Mater. 49 (2001) 3205–3217.
[7] W. Ni, Y.-T. Cheng, D.S. Grummon, Appl. Phys. Lett. 82 (2003) 2811–2813.

[8] X.-G. Ma, K. Komvopoulos, Appl. Phys. Lett. 84 (2004) 4274–4276.
[9] W. Yan, Q. Sun, X.-Q. Feng, L. Qian, Int. J. Solids Struct., in press.
[10] R.H. Richman, A.S. Rao, D. Kung, Wear 181–183 (1995) 80–85.
[11] J. Jin, H. Wang, Acta Metall. Sin. 1 (1988) 76–81.
[12] D.Y. Li, Wear 221 (1998) 116–123.
[13] D.Y. Li, Smart Mater. Struct. 9 (2000) 717–726.
[14] Y.N. Liang, S.Z. Li, Y.B. Jin, W. Lin, S. Li, Wear 198 (1996) 236–241.
[15] K. Kapoor, K.L. Johnson, Proc. Roy. Soc. Lond. A 445 (1994) 367–381.
[16] K. Kapoor, K.L. Johnson, Wear 186–187 (1995) 86–91.
[17] W. Yan, E.P. Busso, N.P. O'Dowd, Proc. Roy. Soc. Lond. A 456 (2000) 2387–2407.
[18] K.L. Johnson, Contact Mechanics, Cambridge University Press, Cambridge, UK, 1985.
[19] J.H. Dautzenberg, J.H. Zaat, Wear 23 (1973) 9–19.
[20] A.W. Ruff, Wear 40 (1976) 59–74.
[21] D.A. Rigney, R. Divakar, S.M. Kuo, Scripta Metall. Mater. 27 (1992) 975–980.
[22] A.T. Alpas, H. Hu, J. Zhang, Wear 162–164 (1993) 188–195.
[23] S. Suresh, Fatigue of Materials, 2nd ed., Cambridge University Press, Cambridge, UK, 1998.
[24] A. Kapoor, Fatigue Fract. Eng. Mater. Struct. 17 (1994) 201–219.
[25] W. Yan, N.P. O'Dowd, E.P. Busso, J. Mech. Phys. Solids 50 (2002) 449–470.
[26] A.L. McKelvey, R.O. Ritchie, Metall. Mater. Trans. A 32 (2001) 731–743.
[27] A. Leyland, A. Matthews, Wear 246 (2000) 1–11.
[28] W.Y. Ni, Y.T. Cheng, M. Lukitsch, A.M. Weiner, L.C. Lev, D.S. Grummon, Wear 259 (2005) 842–848.
[29] K.J.R. Rasmussen, Full-range stress–strain curves for stainless steel alloys, Research report no. R811, Department of Civil Engineering, The University of Sydney, 2001.
[30] W. Yan, C.H. Wang, X.P. Zhang, Y.-W. Mai, Mater. Sci. Eng. A 354 (2003) 146–157.